Simulation of a fully coupled 3D GIA - ice-sheet model for the Antarctic Ice Sheet over a glacial cycle.

Caroline J. van Calcar[1,2], Roderik S.W. van de Wal[2,3], Bas Blank[1], Bas de Boer[4,5], Wouter van der Wal[1,6]

[1]Faculty of Aerospace Engineering, Delft University of Technology, Delft, 2629 HS, The Netherlands
5   [2]Institute for Marine and Atmospheric research Utrecht, Utrecht University, Utrecht, 3508 TA, The Netherlands
[3]Department of Physical Geography, Utrecht University, Utrecht, 3584 CB, The Netherlands
[4]Earth and Climate Cluster, Faculty of Science, Vrije Universiteit Amsterdam, Amsterdam, 1081 HV, The Netherlands
[5]Water Authority Aa and Maas, 's-Hertogenbosch, 5216 PP, The Netherlands
[6]Faculty of Civil Engineering and Geosciences, Delft University of Technology, Delft, 2628 CN, The Netherlands

10   *Correspondence to*: Caroline van Calcar (c.j.vancalcar@tudelft.nl)

Abstract

Glacial Isostatic Adjustment (GIA) has a stabilizing effect on the evolution of the Antarctic Ice Sheet by reducing the grounding line migration that follows ice melt. The timescale and strength of this feedback depend on the spatially varying viscosity of the Earth's mantle. Most studies assume a relatively high laterally homogenous response time of the bedrock. However, 15   viscosity is spatially variable with a high viscosity beneath East Antarctica, and a low viscosity beneath West Antarctica. For this study, we have developed a new method to couple a 3D GIA model and an ice-sheet model to study the interaction between the Solid Earth and the Antarctic Ice Sheet during the last glacial cycle. The feedback effect into account on a high temporal resolution by using coupling time steps of 500 years. We applied the method using the ice-sheet model ANICE, a 3D GIA FE model, and results from a seismic model to determine the patterns in the viscosity. The results of simulations over the Last 20   Glacial Cycle show that differences in viscosity of an order of magnitude can lead to differences in grounding line position up to 500 km, to differences in ice thickness in the order of 1.5 km. These results underline and quantify the importance of including local GIA feedback effects in ice-sheet models when simulating the Antarctic Ice Sheet evolution over the Last Glacial Cycle.

1 Introduction

25   The stability of the Antarctic Ice Sheet (AIS) is largely controlled by the bedrock profile (Pattyn & Morlighem, 2020). The bedrock elevation and slope vary in time due to Glacial Isostatic Adjustment (GIA), which is the response of the solid Earth to a changing ice load. Accurate GIA simulations are needed when analyzing the past and future ice sheet dynamics and stability (e.g. Pan et al., 2021; Gomez et al., 2010). At present, the AIS loses mass in areas where the basal melt increases and the grounding line retreats (Meredith et al. 2019). Fig. 1 shows schematically how GIA affects grounding line migration when 30   the ice sheet retreats. Initially, before ice shelf melting, the ice sheet and bedrock topography are represented by the solid grey and brown lines respectively. The initial position of the grounding line is indicated by p1. Thinning of the ice shelves by

increased basal melting or melt from above, represented by the dashed grey line, leads to a retreat of the grounding line to position p2. Due to a decreasing ice load, the Earth's surface experiences a direct instantaneous elastic uplift and a delayed uplift of the viscoelastic mantle of the Earth, represented by the dashed brown line, causing a local shoaling of water and an

35   outward movement of the grounding line to position p3 (Fig. 1). As a consequence, the GIA feedback slows down migration of the grounding line (Larour et al., 2019; Adhikari et al., 2014; Gomez et al., 2012) and acts as a negative feedback (e.g. Konrad et al., 2015).
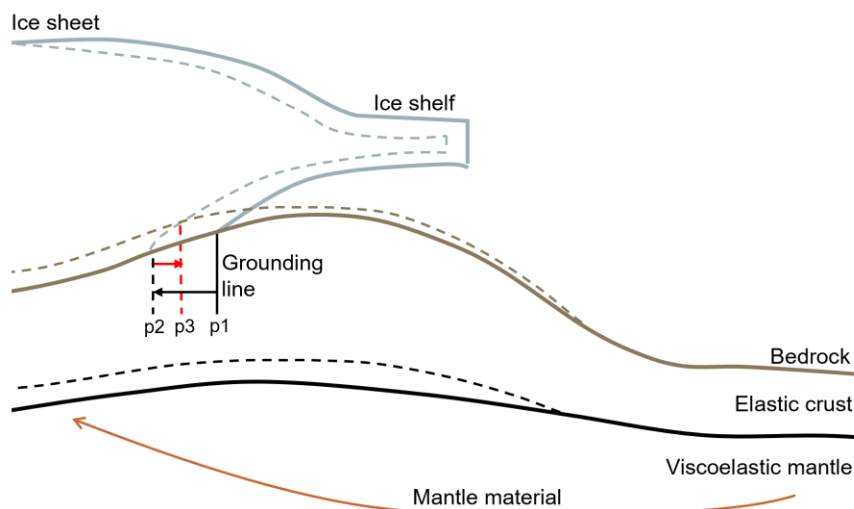

Figure 1: Schematic figure of GIA feedback on grounding line migration. The solid light grey and brown lines represent the initial
40   **ice sheet/shelf and bedrock topography respectively before retreat of the grounding line. The solid black line separates the elastic crust and the viscoelastic mantle. p1 is the grounding line position corresponding to the initial steady state. The dashed light grey line represents the ice sheet/shelf after retreat, the dashed black line is the perturbed mantle elevation, and the dashed brown the new bedrock surface. p2 is the grounding line position after retreat without GIA effects. P3 is the grounding line position after the GIA response.**

45   There exist other GIA feedbacks on the ice sheet evolution apart from the effect on the grounding line. First, the local sea level not only decreases due to bedrock uplift, but also due to the diminishing gravitational attraction of the ice on the surrounding water (e.g. de Boer et al., 2017; Gomez et al., 2015), and due to meltwater flux towards the ocean (e.g. Yousefi et al., 2022). A decrease in sea level in turn enhances uplift from GIA, although to a smaller degree than the loss of grounded ice. Second, GIA could flatten the bed slope, which decreases the rate of basal sliding and ice deformation and therefore decreases the ice

50   flux and ice velocity towards the shelfs (Adhikari et al., 2014). Finally, GIA stabilizes the ice sheet as it reduces the height change of the surface of the ice sheet and thereby suppresses increased melt rates.

Several types of models have been developed to include GIA in ice-sheet models. A basic approach to take changes in bedrock topography into account is using an Elastic Lithosphere Relaxing Asthenosphere model (ELRA) (Le Meur & Huybrechts,

55   1996). This is a two-layer model that contains a local elastic layer and an asthenosphere that relaxes with a single constant relaxation time. This simplified model is computationally cheap and provides a first-order estimate, and is therefore used

widely in ice-sheet models (e.g. Pelletier et al., 2022; de Boer et al., 2017; Pattyn, 2017). However, ELRA assumes a radially and laterally homogeneous flat Earth while the Earth properties vary spatially. Additionally, ELRA neglects the size dependency of the Earths response to ice loading.

60

ELRA has been improved by coupling the lithosphere with a viscous half-space, where viscosity can be used as input parameter instead of the relaxation time (Albrecht et al., 2020; Bueler et al., 2007). Another approach to compute GIA are self-gravitating visco-elastic (SGVE) spherical Earth models. They compute the response to global ice sheet thickness changes with radially varying Earth models, labeled 1D GIA models, that account for gravity field perturbations and displacements using spherical

65   harmonics (e.g. Nield et al., 2014; Whitehouse et al., 2012). Some 1D GIA-sea level models also account for relative sea level change (DeConto et al., 2021; Larour et al., 2019; Pollard et al., 2017; Konrad et al., 2015; de Boer et al., 2014; Gomez et al., 2013). For Antarctica, these 1D GIA models commonly use an Earth structure with a strong upper mantle viscosity of 10^{20}-10^{21} Pa·s and a lithosphere of ~100 km thick which is close to the global average (Geruo et al., 2013). The present-day ice surface elevation resulting from a coupled 1D GIA – ice-sheet model is, for Antarctica, in agreement with the ELRA approach

70   with a relaxation time of 3000 years (Pollard et al., 2017; Le Meur & Huybrechts, 1996), although for the Eurasian ice sheet, the ELRA model with a relaxation time of 3000 years underestimates the Last Glacial Maximum (LGM) ice volume by 30 % (van den Berg et al. 2008).

Even 1D GIA models are oversimplified for Antarctica, as it can be derived from seismic data that the viscosity of the mantle

75   under the AIS varies laterally with six orders of magnitude with much lower viscosities ~10^{18} Pa·s in West Antarctica than the generally assumed global average viscosity (Hay et al., 2017; van der Wal et al., 2015; Ivins et al. 2021). In these low viscosity regions, the Earth's mantle approaches isostatic equilibrium one to two orders of magnitude faster than the timescale of 3000 years that is commonly used in the application of ELRA models (Whitehouse et al., 2019; Barletta et al., 2018). This can be overcome by 3D GIA models which have been developed to simulate GIA using a lateral variable rheology in Antarctica

80   (Blank et al., 2021; Powell et al. 2021; Nield et al., 2018; Hay et al., 2017; van der Wal et al., 2015; A et al., 2013; Geruo et al., 2013; Kaufmann et al., 2005), but they neglect the GIA feedback on the ice sheet evolution because they use a predefined ice sheet history. The only model that coupled 3D GIA with ice dynamics has been developed by Gomez et al. (2018), who show significant differences in ice thickness of up to 1 km in the Antarctic Peninsula and the Ross Sea when a 3D Earth rheology was used instead of a 1D rheology. It can be concluded that uplift is typically underestimated in West Antarctica and

85   overestimated in East Antarctica when using lateral homogenous Earth structures in ELRA or 1D GIA models (Nield et al., 2018).

Coupled GIA – ice-sheet models need an iterative method to include the GIA feedback since ice-sheet models need bedrock deformation as input to compute the ice thickness and GIA models need ice thickness as input. Gomez et al. (2018) applied

90   the following iteration method to simulate the AIS evolution from 40 kyear to present-day. First, the 3D GIA model, including

relative sea level, computes bedrock elevation changes relative to the geoid at time steps of 200 years for the entire 40 kyear using ice thickness changes from a previous coupled 1D GIA simulation. These bedrock elevation changes are corrected at each time step for the difference between the simulated present-day bedrock topography and the observed present-day topography. The corrected bedrock elevation changes are passed to the ice-sheet model to recompute the ice thickness history

95 for the entire period of 40 kyears till present-day with time steps of 200 years. Finally, the new ice thickness history is passed to the 3D GIA model and the process is repeated until the ice and bedrock elevation histories converge. Typically, only four iterations are needed. However, both models are still simulated over the entire period of 40 kyears with a fixed ice or bedrock elevation history as input. Therefore, the time step of the coupling is 40 kyears. Yet, for example in the Amundsen Sea embayment in West Antarctica, GIA occurs on decadal to centennial timescales (Barletta et al., 2018). Present-day GIA

100 estimations and the evolution of the ice sheet could therefore be improved by including the 3D GIA feedback in a coupled model at coupling time steps shorter than 40 kyears.

This study presents a method to fully couple an ice-sheet model and a 3D GIA model on century to millennial timescales from the previous interglacial to present. The method simulates the 3D GIA feedback by iterating an ice-sheet model and a 3D GIA

105 model at every single coupling time step. The method is applied using the ice-sheet model ANICE (de Boer et al. 2013), and a 3D GIA FE model (Blank et al., 2021), where the coupling time step varies over time between 500, 1000 and 5000 years. The coupling method can also be applied with a different ice-sheet model or GIA model. The ice-sheet model is applied to Antarctica to assess the impact of the stabilizing GIA effect on the AIS evolution over the last glacial cycle using 1D and 3D Earth structures. In this study we neglect the spatial variations in sea level.

110

We assess whether widely used 1D Earth structures, for example in Pollard et al. (2017), yield similar stability characteristics for ice sheet evolution caused by bedrock uplift, as 3D Earth structures during the deglaciation phase. The model has potential to improve GIA estimates, and hence corrections for ongoing GIA to geodetic data (e.g. Scheinert et al., 2021; Shepherd et al., 2018). The method cannot only be applied to improve glacial-interglacial ice sheet histories, but also for projections of the

115 AIS evolution.

2 Method

In this section we introduce the ice-sheet model and the GIA model used for this study. After that, we discuss the interpolations that are necessary to feed the ice-sheet model output to the GIA model and the GIA model output to the ice-sheet model. Finally, we describe the coupling method.

2.1 Ice-sheet model: ANICE

The ice-sheet model ANICE is a global 3D ice-sheet model allowing to simulate the AIS, Greenland ice sheet, Eurasian ice sheet and North American ice sheet individually or simultaneously on different equidistant grids for each ice sheet (de Boer et al., 2013). The horizontal resolution is typically 20 km for Greenland and 40 km for the other regions. ANICE has been used for a variety of experiments (Berends et al., 2019; Berends et al., 2018; Bradley et al., 2018, de Boer et al., 2017; Maris et al., 2014; de Boer et al., 2013). Atmospheric temperature and global mean sea level (GMSL) act as the main forcing for the ice-sheet model, as is shown in Fig. S.1 (Van de Wal et al., 2011). The mass balance of the ice sheet is computed using present-day monthly precipitation as a function of the free atmospheric temperature (Bintanja et al., 2005; Bintanja & van de Wal, 2008). A time and latitude dependent surface temperature-albedo-insolation parameterization is used to calculate ablation (Berends et al. 2018). Insolation changes are based on the solution by Laskar et al. (2004). The Shallow Shelf Approximation (SSA) (Bueler and Brown, 2009) is used to solve mechanical equations to determine sliding and velocities of ice shelves, and the Shallow Ice Approximation (SIA) is used to compute velocities of grounded ice (Morland, 1987; Morland & Johnson, 1980). Basal sliding follows a Weertman friction law where friction is controlled by bed elevation. The position of the grounding line determines whether ice is grounded or floating, thus whether the ice experiences sub-shelf melt or not. GMSL and a combination of the ocean temperature-based formulation by Martin et al. (2011) and the glacial-interglacial parametrization by Pollard and DeConto (2009) are used to compute sub-shelf melt. Besides the effect of GMSL, there is an effect from regional sea level variations as well. The effect of the northern hemisphere ice sheets on GMSL is significant but is similar throughout Antarctica (Gomez et al., 2018). The effect of the AIS itself on regional sea level is more important. At regions where grounded ice melts, such as the Ross and the Filchner-Ronne Ice Shelfs during the deglaciation phase, the increase in sea level is reduced due to the decreasing gravitational attraction between the ice sheet and the ocean. However, the effect of regional sea level variations is a second order effect compared to the GMSL variations of all four ice sheets over the last glacial cycle and is therefore not yet included in this model.

The standard version of ANICE uses the ELRA method to compute bedrock elevation changes using a uniform relaxation time that is usually taken to be 3000 years. For this study, ANICE is adjusted to include the bedrock deformation computed by a GIA FE model at coupling time steps of 500, 1000 or 5000 years (see section 2.4.2 for explanation of the chosen coupling time steps). The initial topography at 120 kyears before present is taken from ALBMAP (Le Brocq et al., 2010). Within one coupling time step, the bedrock elevation is updated in ANICE at time steps of 1 year, hereafter referred to as the ANICE time step, using linear interpolation of the deformation computed by the GIA FE model:

$$H_{b,t} = H_{b,t0} + \frac{dH_b}{dt}, \tag{1}$$

where $H_{b,t}$ refers to the updated bedrock elevation at the ANICE time step, $H_{b,t0}$ refers to the bedrock elevation at the beginning of the coupling time step, and $\frac{dHb}{dt}$ refers to the total deformation of one coupling time step computed by the GIA FE model divided by the length of the coupling time step in years. Linear interpolation introduces inaccuracy of the true GIA deformation

which generally follows an exponential curve. Therefore, the deformation would be slightly overestimated at the beginning of the coupling time step. This effect is higher at regions with a lower viscosity of the Earth's mantle due to the increased

155   nonlinearity of the Earths response compared to higher viscosity regions. The effect of this approximation can be reduced by reducing the length of the coupling time step as is shown in section 2.4.2.

2.2 GIA FE model

A FEM model from Blank et al. (2021) is used, which is based on the commercial FEM software ABAQUS (Hibbitt et al., 2016) following Wu (2004). It computes bedrock changes for surface loading on a spherical Earth. The FEM approach allows

160   for discretization and computation of stresses and the resulting deformation in the Earth using a modified stiffness equation and Laplace's equation (Wu, 2004). The advantage of this FEM approach based on ABAQUS is its flexibility: grid size and rheology can be adjusted, and FE models operate in the time domain so the program can be stopped at each time step and all information about the state of stress is stored, on the contrary to SGVE models which operate in the Laplace domain for which the entire ice history has to be stored (e.g. de Boer et al., 2014). FE models can therefore exchange information with the ice-

165   sheet model at each time step. This advantage allows, for example, to simulate the glaciation phase of the last glacial cycle once on a high spatial and temporal resolution, and to use the state of the Earth at the end of the glaciation phase as a starting point for different experiments of the deglaciation phase where, for example, the coupling step size or the forcing of the ice-sheet model is adjusted.

170   The adopted 3D GIA model from Blank et al. (2021) used a prescribed ice load history for all time steps in the model and iterates several times over the full glacial cycle to include self-gravity (Wu, 2004). However, restarting with a different ice load at each coupling time step is necessary to include the GIA-feedback on the ice dynamics. Adjustments to the GIA FE model were made, to be able to continue the GIA FE model with a new ice load after each coupling time step using the RESTART option in Abaqus. For this study, two iterations are performed at each time step to include self-gravity before

175   moving on to the next time step. The same iteration within each time step can later be used for the sea level equation that was included in the original model (Blank et al., 2021) and rotational feedback (Weerdesteijn et al., 2019).

The applied changes in surface loading are relative to the present-day ice load, as it is assumed that the Earth was in isostatic equilibrium with present-day ice loading at the beginning of the last glacial cycle. The surface load is computed at each timestep

180   by computing grounded ice thickness above floatation, taking into account water dumping due to local bathymetry, and the relative sea level change, as described in Simon et al. (2010). The surface load is computed by ANICE using:

$$H_{i,AF} = H_i - \max\left(0, (SL - H_b) \cdot \frac{\rho_w}{\rho_i}\right) \tag{2}$$

where $H_{i,AF}$ refers to the ice thickness above floatation of grounded ice, H_i to the ice thickness of grounded ice, SL to the sea level, H_b to the bedrock elevation, and ρ_w and ρ_i to the density of water and ice respectively. The change in surface load is

185 applied as linear change on the GIA FE model during each coupling time step. This is an approximation of the true ice dynamics over the coupling time step, of which the ice dynamic equations are solved on shorter timescales (1 year) than the coupling time steps and are nonlinear. The determination of the chosen coupling time steps of 5000, 1000 and 500 years is described in section 2.4.2. Not only ice loading causes deformation, but also ocean loading. We conducted a test where we prescribed global loading changes caused by other ice mass changes, taken from Whitehouse et al. (2012), in addition to loading from the

190 Antarctic ice-sheet model. Whereas the effect of global ocean and ice loading could be important on the scale of individual glaciers, the load of relative sea level from other ice mass changes was negligible compared to the ice load variations on the scale of the AIS. Loading due to spatial variations in the sea-level, and due to variations in Earth's rotation, are not considered, as this paper focuses on the direct effect of viscosity.

2.2.1 Model setup and resolution

195 In the GIA model adopted for this study, referred to as the GIA FE model (Blank et al., 2021; Hu et al., 2017), a different viscosity can be assigned to each element which allows for the use of 3D Earth structures (van der Wal et al., 2015). Other parameters (density, Youngs modulus) are taken constant in layers that represent the core, lower and upper mantle and the elastic crust. The horizontal grid is irregular and sensitivity tests are conducted for the trade-off of accuracy versus the computation time. The tests show that using a resolution of 15 by 15 kilometers instead of 30 by 30 kilometers decreases the

200 deformation with 2 cm over 1000 years and increases the computation time by approximately 30 percent to 15 minutes (Fig. S.2). Since the difference in deformation is insignificant, an approximate resolution of 30 by 30 km is chosen at the surface in Antarctica from 62 degrees latitude to the south pole, and 200 by 200 km elsewhere. Since the grid lies on a sphere, the elements are not equal, but their size approaches the given resolution. The resolution in the lower mantle is double as coarse as the lithosphere and the upper mantle. The chosen resolution results in approximately 300,000 elements divided over several

205 layers, where the crust and upper mantle have double the elements of the lower mantle and the core. The FE model is divided in eight layers for the 1D simulations and 9 layers for the 3D simulations to represent the upper and lower mantle so that the elements in each layer lie at the same depth. The bottom of the upper mantle is connected to the lower resolution lower mantle with the use of so-called tie constraints. Fig. 2 shows an example of a change in a deformed sphere due to ice loading at East Antarctica and ice unloading at West Antarctica, with a relatively high-resolution in and around Antarctica and lower resolution

210 in the far-field.
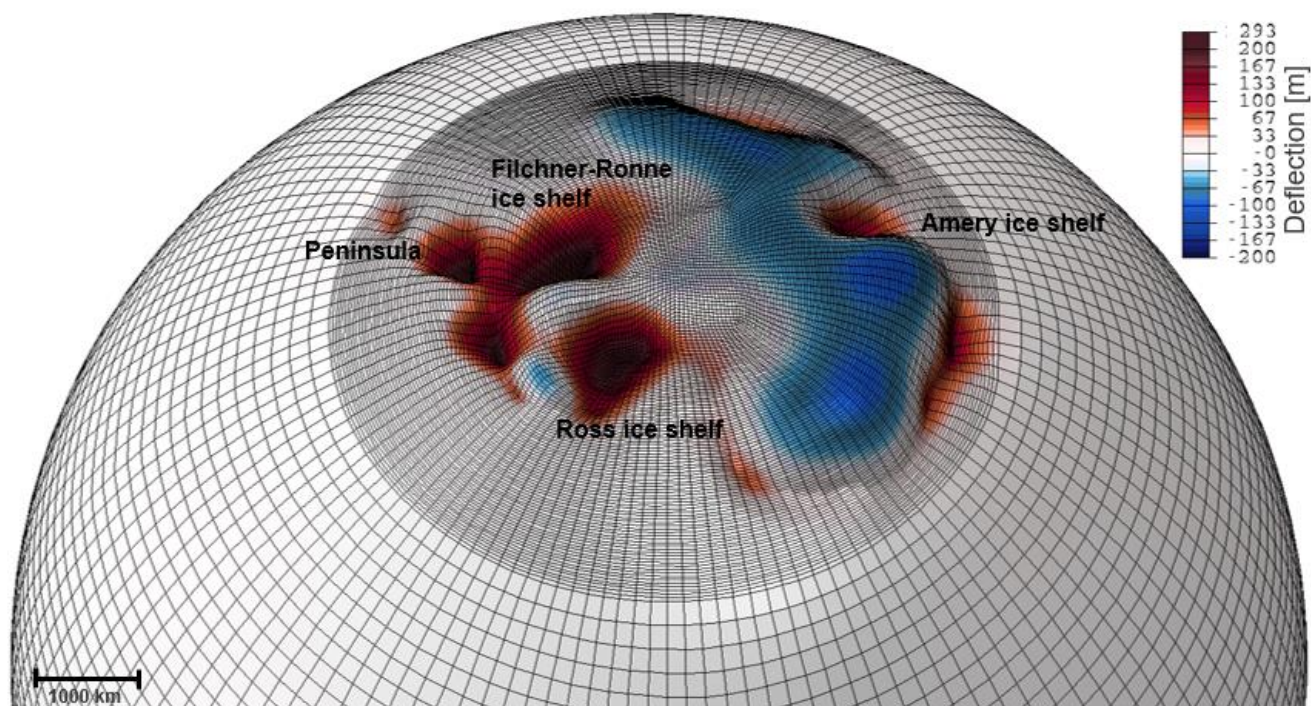
Figure 2: Example of the deformed Earth simulated by the GIA FE model at 115 kyears before present. The grid has a higher resolution area of 30 by 30 km at latitudes until -60 degrees, and a lower resolution area of 200 by 200 km above -60 degrees latitude. The ice sheet is mainly growing in West Antarctica, causing downward deformation (positive deflection), and slightly decreasing in East Antarctica which causes uplift (negative deflection).

Following the 5-layer model used in Spada et al. (2011), a density, Young's modulus and, in the case of a 1D model, a viscosity is assigned to each layer. The chosen viscosities of $5 \cdot 10^{21}$ and 10^{21} Pa·s for the mantle between 420 and 2891 km depth are consisted with GIA based inferences of radial viscosity (Lau et al., 2016; Lambeck et al., 2014). In case of a 3D Earth structure, the elastic top layer is fixed till 35 km depth as this is the thinnest lithosphere found in West Antarctica (Pappa et al., 2019), and a 3D rheological model with specific dislocation and diffusion creep parameters is assigned to each element between 35 and 670 km depth, as is described in section 2.2.2. The effective viscosity determined by these parameters will lead to a thicker effective lithosphere than 35 km in most of Antarctica. The overview of the parameter set up is shown in Table 1.

8

Table 1: Material properties of the GIA model. The top of upper mantle 2 is at 100 km depth for the 1D simulation and at 35 km for the 3D simulation.

Earth layer	Depth [km]	Number of FE layers in model	Density [kg/m³]	Young's modulus [Pa]	Viscosity [Pa·s]
Crust	0 - 35[(3D)]/100[(1D)]	1	3037	$0.50605 \cdot 10^{11}$	$1 \cdot 10^{44}$
Upper mantle 1	35[(3D)]/100[(1D)] – 420	3/4	3438	$0.70363 \cdot 10^{11}$	1D/3D variable
Upper mantle 2	420 - 670	2	3871	$1.05490 \cdot 10^{11}$	$1 \cdot 10^{21}$
Lower mantle	670 - 2891	2	4978	$2.28340 \cdot 10^{11}$	$5 \cdot 10^{21}$
Core	2891 - 6371	1	10750	$1 \cdot 10^{-20}$	0

2.2.2 Rheology and seismic models

The deformation as a result of the applied ice load is dependent on the rheological model that is used by the GIA FE model. Rheological models describe the relation between stress and strain. The 1D version of the GIA FE model uses a linear Maxwell rheology at all depths, whereas the 3D version uses a composite rheology following van der Wal et al. (2010) at depths between 30 and 420 km. The composite rheology combines two deformation mechanisms, diffusion and dislocation creep such that the strain computed in ABAQUS is:

$$\Delta\epsilon_{ij} = \frac{3}{2}\left(B_{diff} + B_{disl}\tilde{q}^{n-1}\right)q_{ij}\Delta t, \tag{3}$$

where $\Delta\epsilon_{ij}$ is the strain, B_{diff} and B_{disl} are the spatially variable diffusion and dislocation parameters respectively, $\tilde{q}$ is the Von Mises stress which is assumed to be 0.1 MPa (Ivins et al., 2021), n is the stress exponent, taken to be 3.5, consistent with Hirth and Kohlstedt (2003), q_{ij} is the deviatoric stress tensor, and Δt is a variable time increment for the numerical integration within the coupling time step. The increments are determined automatically depending on the applied stress and the size of the coupling time step. Detailed explanation of the implementation of the composite rheology in the FE model can be found in Blank et al. (2021).

From Eq. 3 it can be derived that the effective viscosity (η_{eff}) for each element of the GIA FE model (van der Wal et al., 2013) becomes:

$$\eta_{eff} = \frac{1}{3B_{diff} + 3B_{disl}q^{n-1}}, \tag{4}$$

The diffusion and dislocation parameters used in this study are derived from the flow law from Hirth and Kohlstedt (2003) and given by Eq. 5a and 5b respectively:

$$B_{diff} = A_{diff}d^{-3}f_{H_2O}^1 e^{-\frac{E+PV}{RT_{x,y}}}, \tag{5a}$$

$$B_{disl} = A_{disl}d^0 f_{H_2O}^{1.2} e^{-\frac{E+PV}{RT_{x,y}}}, \tag{5b}$$

where A is experimentally determined, d is the grain size, f_{H_2O} is the water content, E is the activation energy, P is the depth dependent pressure (Kearey et al., 2009), V is the activation volume, R is the gas constant and Tx,y is the spatially variable absolute temperature. A, E and V are different for wet and dry olivine. All parameters, except temperature, grain size and water content, are taken from Hirth and Kohlstedt (2003). The temperature is derived from an Antarctic seismic model and a global

255 seismic model for each element of the GIA FE model following approach 3 in Ivins et al. (2021). Seismic velocity anomalies are converted to temperature, assuming that all seismic velocity anomalies are caused by temperature variations (Goes et al., 2000). Derivatives of seismic velocity anomalies to temperature anomalies are provided as a function of depth of the mantle (Karato et al., 2008). Antarctic seismic velocity anomalies are taken from Lloyd et al. (2020) and global velocities anomalies for regions above -60 degrees latitude are taken from SMEAN2 which is an average of three seismic models (Becker & Boschi,

260 2002). The models are combined with a smoothing applied at the boundary at -60 degrees latitude. Mantle melt is assumed to have a relatively small influence on upper mantle viscosity and is therefore not included in this study (van der Wal et al., 2015).

Following Eq. 3-5, the viscosity, and thus the deformation, is dependent on the grain size and water content. As little information exists on grain size and water content, these parameters are kept spatially homogeneous (van der Wal et al., 2015).

265 We obtained two different 3D rheologies by choosing a grain size of 4 mm and a water content of 0 (hereafter referred to as 3Ddry) and 500 ppm (hereafter referred to as 3Dwet) to obtain rheologies that can be considered realistic based on other viscosity studies (e.g. Blank et al., 2021; Gomez et al., 2018; Hay et al., 2017). A water content of 500 ppm is within the range of water content found in Antarctic xenoliths (Martin, 2021).

270 The two models give an idea of some, though not all, variation in 3D viscosity. The viscosity of both 3D rheologies is shown at three depths in the two right columns of Fig. 3. Increasing the water content lowers the viscosity but the pattern of viscosity variations is maintained (Karato et al., 1986; Blank et al., 2021). This can be seen in Fig. 3, where the viscosity of 3Ddry is approximately one order of magnitude higher than the viscosity of 3Dwet. Both 3D rheologies provide an upper mantle viscosity of approximately 10^{18} Pa·s in West Antarctica, which is comparable with Barletta et al., (2018), who estimated such

275 low viscosities in West Antarctica by constraining the GIA model using GPS and seismic measurements, and with Blank et al. (2021), who confirmed that a viscosity of 10^{18-19} Pa·s is plausible in the Amundsen Sea sector, based on the WINTERC 3.2 temperature model which is constrained by seismic data and satellite gravity data (Fullea et al., 2021). The viscosity pattern of both 3D rheologies used in this study, and the viscosity value of the 3Ddry rheology, are similar to the viscosity used by Gomez et al. (2018) and Hay et al. (2017), who obtained viscosity by scaling seismic anomalies to viscosity anomalies and adding

280 them to background viscosity profile from GIA or geodynamic studies. A background viscosity can be obtained from other GIA or geodynamic studies, however following the method from van der Wal et al. (2015) allows to directly obtain absolute viscosity values from seismic measurements, assuming only a temperature profile and not a viscosity profile.

The results of the coupled model using a 3D rheology can be compared with the results using 1D rheologies. Two experiments
285 are performed using a 1D rheology with an elastic lithospheric thickness of 100 km and an upper mantle viscosity of 10^{20}
(hereafter referred to as 1D20) and 10^{21} Pa·s (hereafter referred to as 1D21), consistent with the lower and upper boundaries
of the upper mantle viscosity that is generally used in studies for Antarctica (e.g. Albrecht et al., 2020; Pollard et al., 2017;
Gomez et al., 2018). The viscosity of the 3D rheologies are up to 4 orders of magnitude lower in West Antarctica and up to 3
orders of magnitude higher in East Antarctica compared to the 1D21 rheology. Therefore, the rheology is generally weaker in
290 West Antarctica and somewhat stiffer in East Antarctica in the 3D rheologies compared to the 1D rheologies.
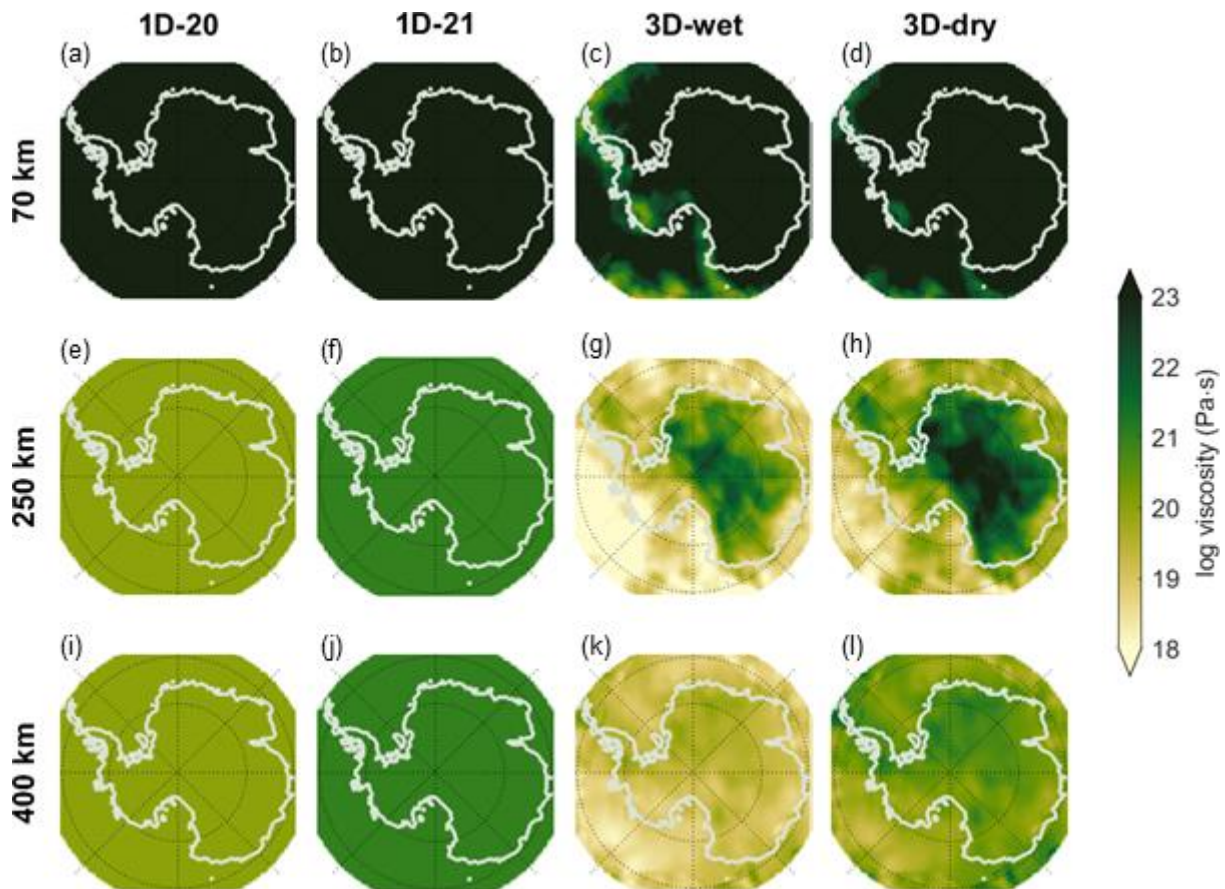

**Figure 3: Panels a, e and i correspond to the 1D rheology referred to as 1D20. Panels b, f and j correspond to the 1D rheology
referred to as 1D21. Panels a and b show a viscosity of 10^{44} Pa·s, representing the 100 km thick lithosphere in the 1D rheology. Panels
295 c, g and k correspond to a 3D rheology with a water content of 500 ppm referred to as 3D (wet), and figures d, h and l correspond
to a 3D rheology without water content referred to as 3D (dry). Both 3D rheologies assume a grain size of 4 mm. A pressure of 0.1
MPa is used to compute the viscosity from the dislocation and diffusion parameters.**

2.3 Interpolation of bedrock deformation and ice loading

The total deformation computed by the GIA FE model that is used as input for ANICE, is defined on a regular grid of 0.25 by
300 0.25 degrees, whereas ANICE is defined on a polar stereographic equidistant grid of 40 km. Therefore, interpolation of the

11

output is needed to use the output of the GIA FE model as input for ANICE. On the other hand, interpolation of the ANICE output is needed to use the output as input for the GIA FE model. For both interpolations we use Oblimap (Reerink et al., 2016). For interpolation from the fine grid size of the GIA FE model to a somewhat coarser grid size of ANICE, the so-called radius method is used as this is computationally fast and provides an accurate result (Reerink et al., 2016). All fine grid points within a radius of the order of half the coarse grid size are included by a Shepard distance-weighted averaging interpolation method to obtain a representative value for this coarse grid point (Shepard, 1968). The quadrant method is used for gridding from a coarser ANICE grid to a somewhat finer grid of the GIA FE model (Reerink et al., 2016). The region around the grid point of the fine grid is divided in four quadrants. For each quadrant, the closest grid point is selected and shepard distance-weighted averaging is applied to these grid points using a Shepard's power parameter of 2 (Shepard, 1968). A lower parameter would result in a smoother output but also less detail. Furthermore, the ice thickness is linearly interpolated from the regular input grid of 0.25 degrees latitude by 0.25 degrees longitude to the irregular grid of the actual GIA FE sphere.
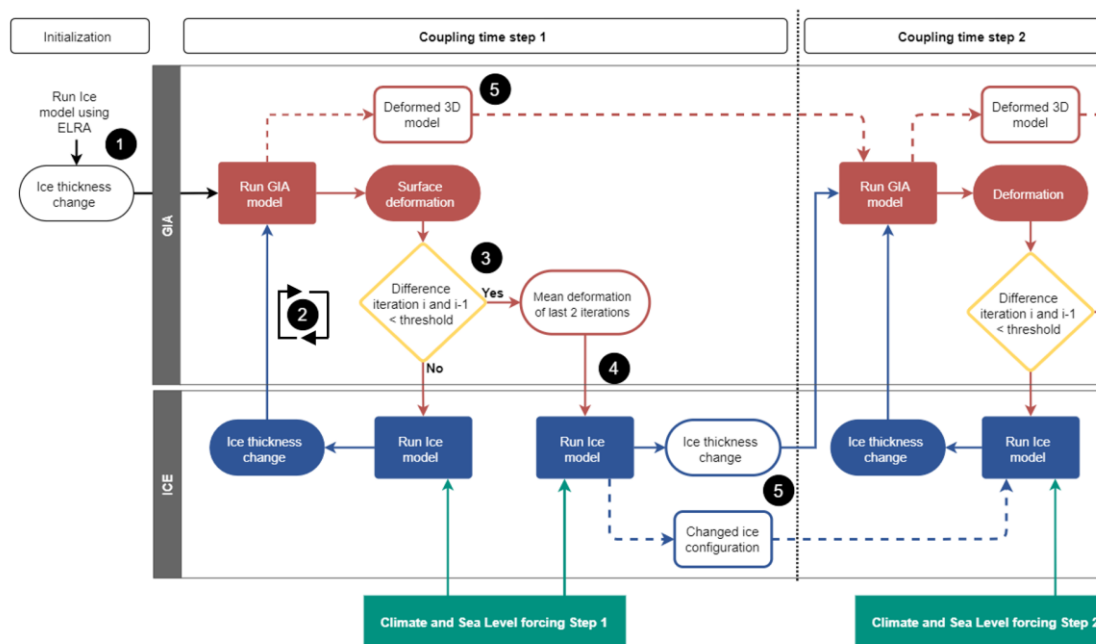
2.4 Iterative coupling method

The simulation of ice dynamics for a certain coupling time step requires the deformation of the Earth over the coupling time step. On the other hand, the computation of the deformation over this coupling time step, using the GIA FE model, requires the change in ice mass over that coupling time step. For this study, an iterative coupling scheme has been developed that alternates between the models per time step of 500 to 5000 years. The iterative scheme is shown in Fig. 4. The ice thickness and deformation at each coupling time step of the coupled model is computed as follows:

1. Simulate the evolution of the AIS for the first coupling time step using ELRA. Use the difference in grounded ice thickness at the end of the coupling time step and the initial grounded ice thickness as input for the GIA FE model which starts initially in isostatic equilibrium.

2. Run the GIA FE model to compute the deformation of the Earth's surface during the first coupling time step. Pass the total deformation to the ice-sheet model. Run the ice-sheet model to compute the new ice sheet evolution at the first coupling time step using the updated deformation in linear increases during the coupling time step.

3. Continue the iterative process described in step 2 until a convergence criterium has been reached. The convergence of the coupled model and the required number of iterations is further described in section 2.4.1.

4. Take the average deformation of the last two iterations as the final deformation to minimize the uncertainties in areas where the coupled model does not converge to zero but alternates between positive and negative values. Pass the average deformation to the ice-sheet model and run the model to calculate the final ice sheet evolution over the first coupling time step.

5. All stresses present at the end of the first coupling time step are saved in the GIA FE model. The final configuration of the ice-sheet model at the end of the first coupling time step is the starting point for the ice-sheet model simulation

at the second coupling time step. The averaged deformation of the last two iterations of the previous coupling time step will be used as initial guess to run the ice-sheet model for the first iteration of the next coupling time step.

Figure 4: Schematic overview of the method for coupling the GIA and ice-sheet model. The numbers 1 to 5 in black circles refer to the steps of the iterative coupling process explained in the main text.

Gomez et al. (2018) creates ice loading and bedrock deformation histories of 40 kyear with a temporal resolution of 200 years and run the ice-sheet model and sea level model alternately at once over the full history. In the method of this study, the ice-sheet model and GIA FE model run alternately at each dynamic coupling time step, of which the coupling time step can be changed depending on the desired accuracy. For this study, the last glacial cycle is simulated using 51 coupling time steps of 5000, 1000 and 500 years (section 2.4.2). Tests are performed to determine the required number of iterations per coupling time step (section 2.4.3). After calculating the first glacial cycle there is a usually a mismatch between modelled and observed topography at present-day. To solve this mismatch, we use three to four glacial cycle iterations, depending on the rheology, to correct for the difference (section 2.4.4) (Kendall et al., 2005). The method allows to use variable coupling time steps throughout the glacial cycle and between iterations of glacial cycles to decrease the total computation time.

2.4.1 Convergence of the coupled model

The coupled model requires three iterations per coupling time step to converge to an incremental change in deformation of less than 0.5 mm per year when using the 1D21 rheology. The exact number of iterations needed to convergence is dependent on the change in ice load. An example of convergence of a coupling time step can be seen in Fig. 5, which shows the difference in deformation and ice thickness between iterations of one coupling time step from 120 kyear till 115 kyear before present.

Panel a of Fig. 5 shows the change in ice thickness and panel b shows the change in bedrock elevation over this coupling time step. Panels c to f show the difference in ice thickness and bedrock elevation compared to the former iteration. It can be seen that the ice thickness and deformation do not converge exactly at multiple locations around the grounding line after iteration 3. A high deformation rate and large changes in ice thickness cause a large shift in the position of the grounding line. Glaciated grid cells of the ice-sheet model are defined as grounded ice or floating ice, depending on their position upstream or downstream of the grounding line. If the grounding line in the ice-sheet model moves with every iteration due to large changes in deformation, the grid cells around the grounding line alternate between an ice shelf and grounded ice status. Since ice thickness can differ with hundreds of meters between adjacent grid cells, the difference in ice thickness at one grid cell between iterations can also differ greatly. In this case, ice thickness, but also deformation at these grid cells around the grounding line do not converge to exactly zero. The bedrock deformation converges better than ice thickness because of the stiffness of the Earth causing a more smooth deformation pattern. Although convergence to zero cannot be reached everywhere, an alternation of the same negative and positive value is reached for these locations from iteration 2 onwards.

Tests show that the coupled model convergences within an acceptable computation time when the convergence criterium is set to 0.5 mm per year over the coupling time step. This is within the uncertainty range of the GIA FE model, based on uncertainties from the rheological model such as background temperature and seismic velocity (e.g. Blank et al. 2021) and accuracy of paleo sea level records. Since the grid cells around the groundling line often do not converge to zero but to alternating values, the coupling method introduces an uncertainty. For example, if in one grid cell the total deformation over 5000 years keeps alternating between -2 and +2 meter, the uncertainty range is 4 meter. The average deformation of the last two iterations is used as the final deformation to decrease this uncertainty. This average deformation is then used to simulate ANICE for the final iteration of the time step.
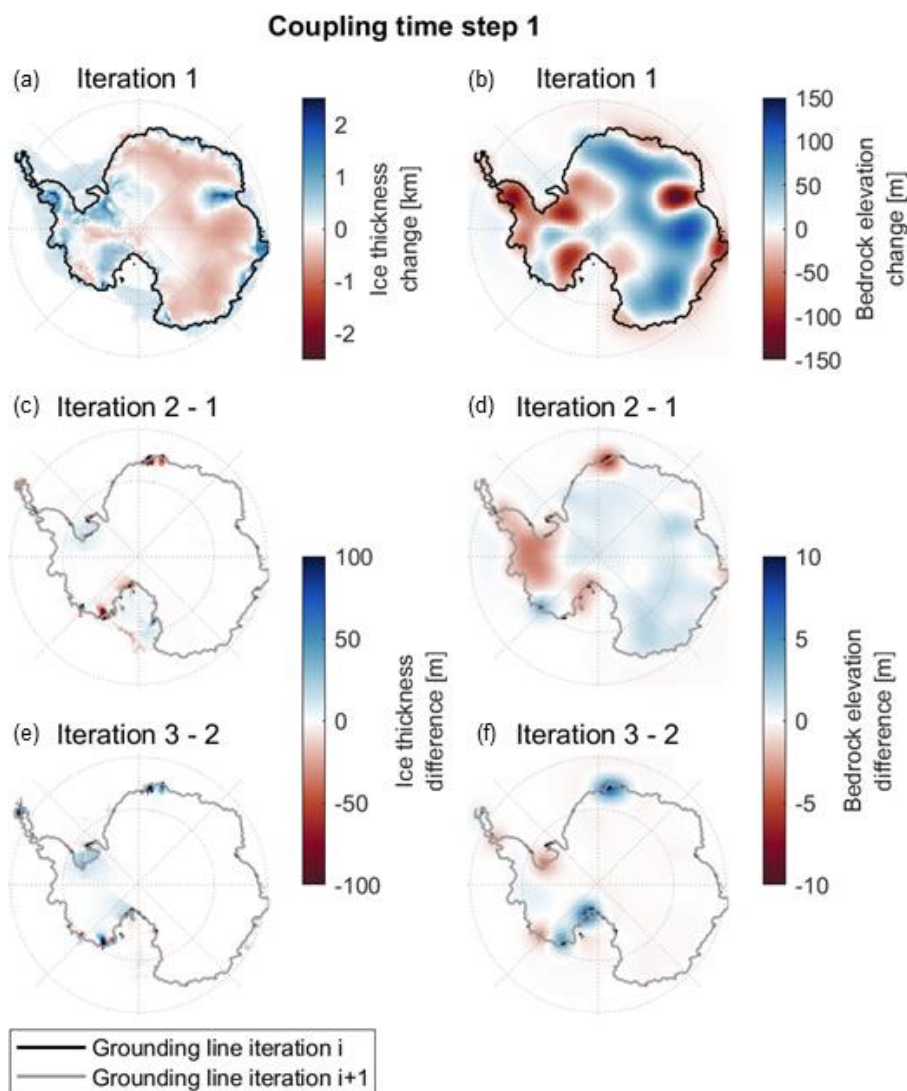
Figure 5: Iterations of coupling time step 1 from 120 kyear to 115 kyear before present. (a) Change in ice thickness over this coupling time step. (b) Change in bedrock elevation over this coupling time step. (c-f) Difference in ice thickness and bedrock elevation change compared to the previous iteration.

2.4.2 Size of the coupling time step

The convergence of the coupled model is highly dependent on the change in deformation and ice thickness over one coupling time step, and therefore also on the length of the coupling time step. A small time step is desirable to increase the number of grid cells converging to zero. Furthermore, the time steps need to be chosen sufficiently small, so that deformation and ice thickness change nearly linearly. On the other hand, a large time step is desirable to limit the computation time. The coupled model is tested using different coupling time steps, leading to a maximum time step of 5000 years and smaller time steps of 1000 and 500 years during the deglaciation phase. The chosen time steps for the entire glacial cycle for this study are shown

385 in Table 2. A time step of 5000 years is chosen between 120 kyears and 20 kyears before present because the change in GIA signal is small within this period since the ice sheet is slowly increasing till LGM, and knowledge of the past climate is limited. Since the change in GIA signal increases due to fast unloading in a warming climate, smaller time steps of 1000 and 500 years were chosen during the deglaciation. Han et al. (2022) showed that coupling time steps of 400 years are optimal for the deglaciation phase using a coupled 1D GIA – ice-sheet model, but their method assumes a constant topography during one

390 coupling timestep which requires smaller timesteps than the coupling method presented in this study.

Table 2: Time steps over last glacial cycle.

Period [kyears before present-day]	Time step size [kyears]
120 – 20	5
20 – 15	1
15 – 5	0.5
5 – 1	1
1 - 0	0.5

2.4.3 Number of iterations per time step

Two simulations are conducted to study the effect of the number of iterations on GIA and the evolution of the AIS using the low viscosity 1D coupled model (1D20). One simulation with 1 iteration per time step, and one simulation with a varying

395 number of iterations per time step using the convergence threshold as described in section 2.4.1. Differences in deformation and ice thickness between the simulation with 1 iteration and the simulation with multiple iterations are always concentrated around the grounding line since the grounding line position can differ between iterations, as is discussed in section 2.4.1. The maximum deformation and ice thickness differences vary per time step. The absolute maximum difference is 1365 meter in ice thickness at one ice sheet grid cell, and 1045 meter at 8 kyears before present at two different grid cells in our simulations.

400 However, these differences can be considered as outliers because the absolute mean of the maximum differences at all grid cells over all time steps is 2.4 meter. The maximum difference in ice thickness at present-day is 5 times smaller than the maximum difference between using different 1D and 3D rheology's and only occurs over very small regions. From this we conclude that the improvement in the performance by applying multiple iterations is insignificant when using the time steps as described in section 2.4.2, and 1 iteration is used for results in the remainder of the paper.

405

Reducing the number of iterations significantly reduces the computation time. The coupled model simulations are performed on 16 CPU's of model Intel(R) Xeon(R) Gold 6140 CPU @ 2.30GHz, of which the CPU speed varies between 1085 and 2707 MHz. A simulation of one glacial cycle using the 1D GIA FE model takes 27 days when running on 16 CPU's performing 51 time steps and 293 iterations in total. Performing only one iteration reduces the total running time to 30 hours. Simulating the

410 last glacial cycle using a 3D GIA FE model takes about 5 days when only 1 iteration per time step is performed, and 37 days when in total 293 iterations are performed.

16

2.4.4 Iterations over the entire glacial cycle

The bedrock elevation at last glacial maximum is higher in case a rheology with a larger viscosity is used since there is less subduction during the glaciation phase. Ice shelfs in West Antarctica will melt less during the deglaciation phase when a stronger rheology is used due to the higher bedrock elevation. At the end of the simulation of one glacial cycle, the present-day topography differs per simulation and does not equal the observed topography. Differences in ice sheet evolution during the deglaciation phase are then mainly caused by a different topography at last glacial maximum rather than differences in rheology. Several iterations of the entire last glacial cycle, hereafter called glacial iterations, are needed to ensure that modelled and observed present day topography are in agreement (Peltier, 1994; Kendall et al., 2005). If they are not, it is assumed that initial topography is in error. It is assumed here that this difference is solely caused by vertical GIA deformation, neglecting other types of deformation, such as tectonic motion and erosion or shortcomings in the ice-sheet model.

The initial topography at 120 kyears before present of the first glacial iteration is initially assumed to be equal to present-day topography, taken from ALBMAP (Le Brocq et al., 2010). For the next glacial iterations, the initial topography is adjusted for the difference in simulated present-day topography and the observed present-day topography ALBMAP:

$$H_{b0,i} = H_{b0,i-1} + (H_{b,ALBMAP)} - H_{bPD,i-1}) , \qquad (6)$$

where, $H_{b0,i}$ refers to the bedrock elevation at the beginning of the new glacial iteration, $H_{b0,i-1}$ refers to the bedrock elevation at the beginning of the previous glacial iteration, $H_{bPD,i-1}$ refers to the present-day bedrock elevation of the last glacial iteration and $H_{b,ALBMAP)}$ refers to the observed present-day topography based on Le Brocq et al. (2010). Four to five iterations of the entire glacial cycle are typically needed to converge the modelled present-day topography to the observed present-day topography, of which the first three iterations are shown in Fig. S.3 in the supplementary materials.

3 Results and discussion

3.1 Testing the coupled model using different 1D rheologies

The evolution of the AIS over the entire last glacial cycle shows a similar ice sheet thickness, extend and volume using the 1D coupled model of this study, compared to other studies using coupled 1D GIA – ice-sheet models and coupled ELRA – ice-sheet models (de Boer et al., 2014, 2017; Gomez et al., 2015; Pollard et al., 2017). To further test if the coupled model works as expected, the results for an upper mantle viscosity of 10^{20} Pa·s (1D20) are compared to those of 10^{21} Pa·s (1D21). These simulations also allow to study the differences between 1D and 3D rheologies as discussed in section 3.2. The results of both simulations in terms of ice thickness and grounding line position follow a similar pattern as in Pollard et al., (2017). The Filchner-Ronne and Ross Ice Shelfs (indicated with FR and R respectively in Fig. 6a) remain larger during the deglaciation phase for the 1D20 simulation than for the 1D21 simulation because the uplift is faster when using the smaller viscosity of

10^{20} Pa·s (Fig. 6). Based on the Marine Ice Sheet Instability (MISI) process, increased ice shelf melt and fast grounding line retreat can be expected due to a retrograde bedrock slope and an increasing relative sea level caused by subsidence (Schoof, 2007). At present day, the ice is up to 1 km thinner around the grounding line of the Ross and Filchner-Ronne Ice Shelfs, and
445   the grounding line is further retreated by approximately 300 km at the Ross Ice Shelf if we compare the 1D21 to the 1D20 results, shown in Fig. 6h.
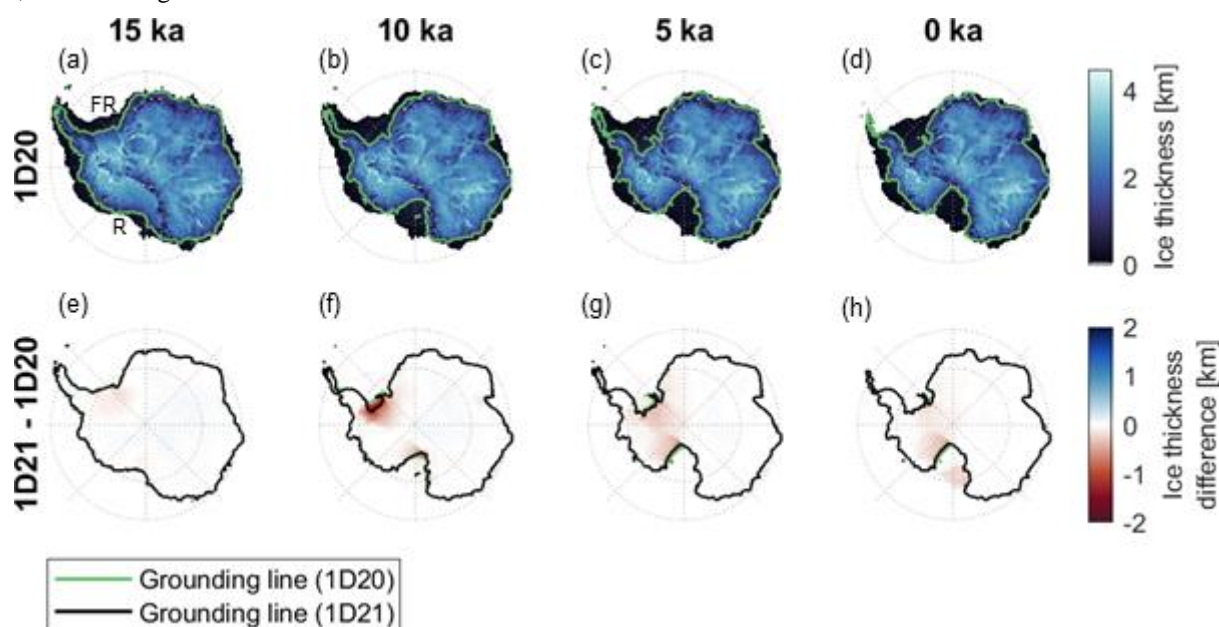
Figure 6: Ice thickness of 1D20 (top row) and the difference in ice thickness between 1D20 and 1D21 (bottom row) at four epochs during the deglaciation phase. (a) FR refers to the Filchner-Ronne Ice Shelf and R refers to the Ross Ice Shelf. In (e-f), the 1D20
450   **grounding line (green) mostly overlaps with the 1D21 grounding line (black).**

3.2 Stabilization of the AIS using 1D and 3D rheologies.

In a cooling climate between 120 kyears and 20 kyears before present, all 1D and 3D coupled simulations show an ice thickness increase mainly at the Ross and the Filchner-Ronne Ice Shelfs and at the Peninsula, causing the bedrock to subside in these regions. In the 1D simulations, the bedrock subsides approximately 500 meter less during this period than in the 3Ddry
455   simulations due to the stiffer 1D rheology compared to the 3D rheology with a difference in viscosity of 2 orders of magnitude. This leads to increased growth of ice until LGM when a 1D rheology is used. At LGM, the ice thickness is several hundreds of meter larger near the Ross and the Filchner-Ronne Ice Shelfs when using a 1D rheology compared to the 3Ddry rheology (Fig. 7a, e and i). During the deglaciation phase, the Ross and Filchner-Ronne Ice Shelfs retreat fast due climate warming, similar to other studies of the AIS evolution suggest (e.g. Albrecht et al., 2020). The 1D viscosity leads to a slower uplift which
460   causes the grouding line near the Ross and Filchner-Ronne Ice Shelfs to retreat faster in the 1D simulations than in the 3D

simulation, corresponding to results by Pollard et al. (2017) and Gomez et al. (2018). Using a 3D viscosity leads to a difference in grounding line position of up to 500 km and a difference in ice thickness of up to 1.5 km at present-day (Fig. 7c, g, k).

465 In contrast to the changes in West Antarctica, Fig. 7 shows that the difference in ice sheet thickness between the 1D and 3Ddry simulations in the interior of the East AIS are not larger than 60 meter, although the viscosity in East Antarctica is several orders of magnitude higher in the 3D rheology than in the 1D rheologies. This is because the interior of the ice sheet is not as sensitive to the bedrock elevation as the outlet glaciers near the margin, leading to an insignificant effect of viscosity differences.
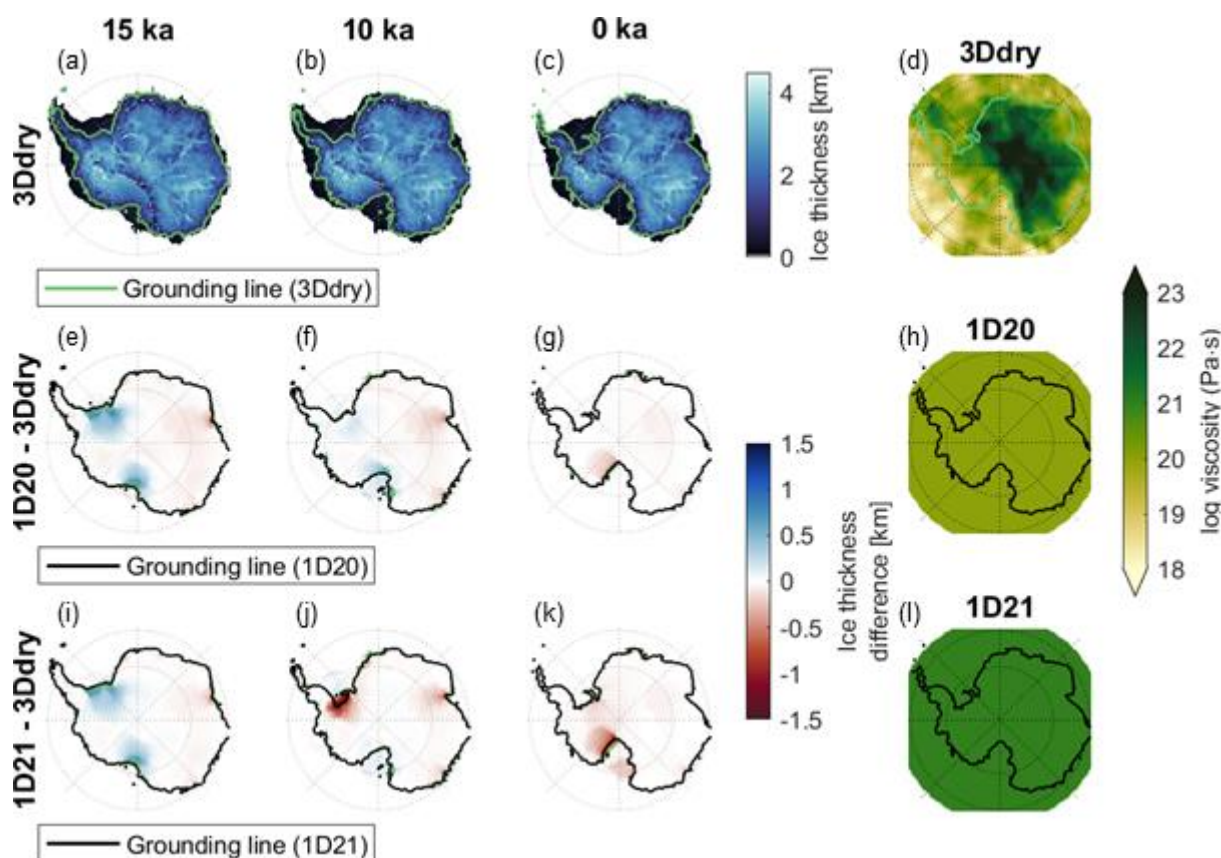

470 **Figure 7: 1D vs 3D ice thickness and viscosity. In Fig6e-g and 6i-k, the 1D grounding lines (black) mostly overlaps with the 3D grounding line (green).**

Two simulations are done to study the sensitivity to different realistic 3D rheologies (Fig. 8). The maximum difference in ice thickness at present-day between the two 3D simulations is 200 meter and the maximum difference in grounding line position is approximately 40 km (Fig. 8.g). The difference in ice thickness and grounding line retreat between 1D simulations and 3D 475 simulations is three times higher than the difference between two 3D simulations. This is caused by the different patterns of

viscosity, which differs 3 to 4 orders of magnitude between the 1D and the 3D rheology and only 1 order of magnitude between the two 3D simulations (Fig. 3).
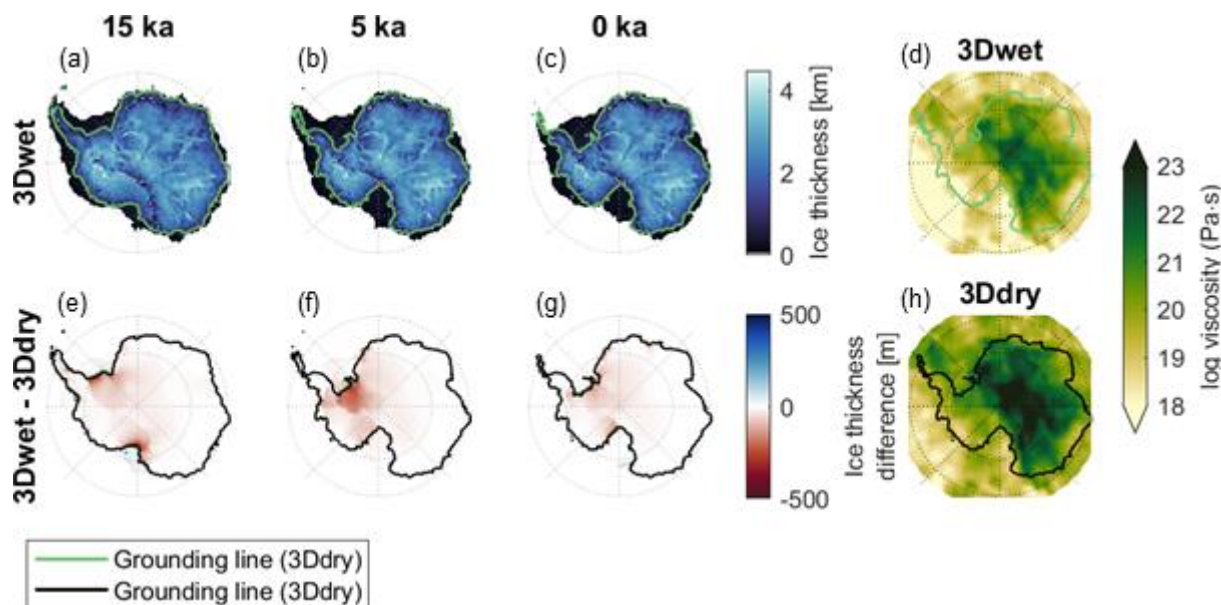
Figure 8: 3D wet vs 3D dry from Last Glacial Maximum till present-day. In (a-c) and (e-g), the 3D dry grounding line (black) mostly overlaps with the 3D wet grounding line (green). (d) and (h) show the 3Dwet and 3Ddry viscosity with the corresponding grounding line at present-day.

Figure 9 shows that the present-day ice volume is 0.6-1.8 m.w.e. lower when using 1D rheologies compared to using 3D rheologies. The use of a 3D rheology stabilizes the ice sheet compared to the use of a 1D viscosity (Fig. 9) because a lower viscosity at West Antarctica stabilizes the Filchner-Ronne and Ross Ice Shelfs (Fig. 8). Gomez et al. (2018) found an insignificant difference in ice volume at present-day. Gomez et al. (2018) included the effect of regional sea level in the coupled model. Including this effect in our model would decrease ice shelf melt and therefore decrease the ice volume change itself and the difference in ice volume between the 1D and 3D simulations. Differences in terms of ice dynamics formulations, forcings, rheology and resolution could possibly explain the different result of Gomez et al. (2018) and this study.
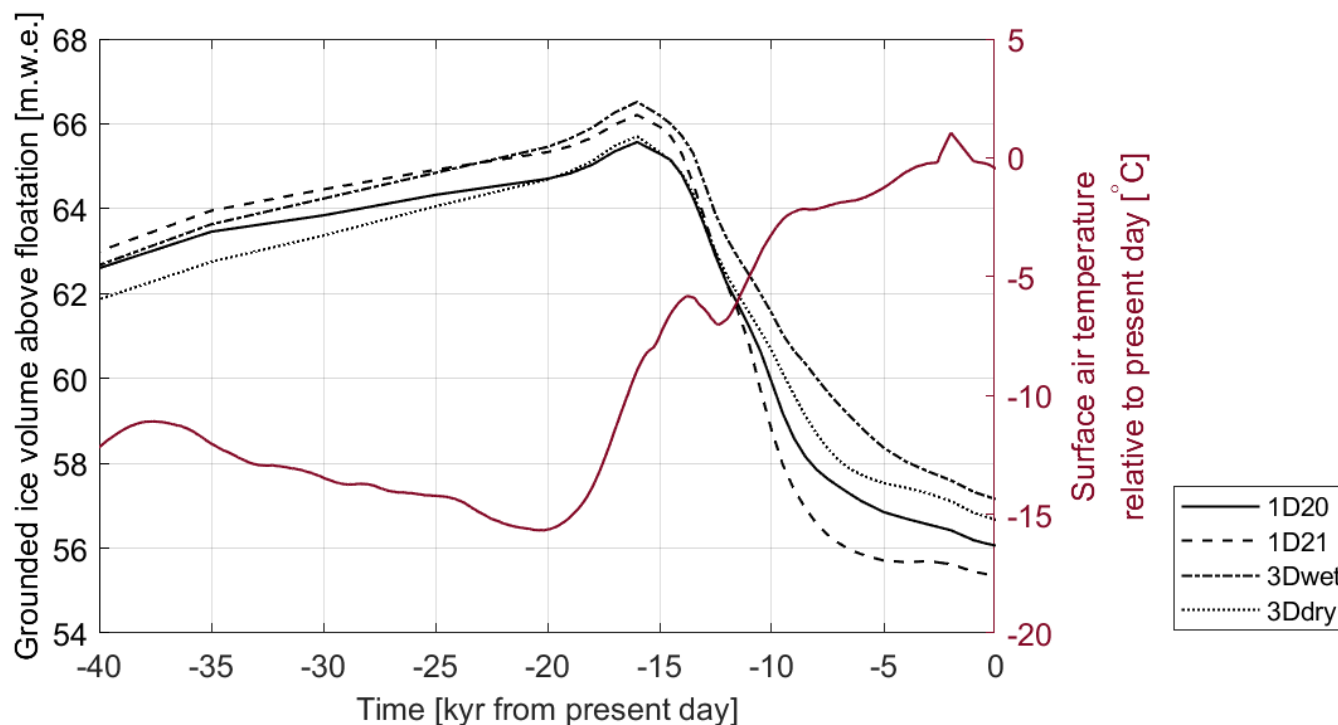
Figure 9: The black lines show the AIS volume over time for the 1D simulations and for the two 3D simulations (dry and wet rheology). The red line shows the mean surface temperature.

Overall, it can be concluded that the variations in viscosity between a realistic 3D rheology and commonly used 1D rheology have a significant impact on grounding line position and ice thickness in West Antarctica and an insignificant impact in East Antarctica. Furthermore, the difference in ice thickness of the 3Ddry and the 1D20 simulations is smaller than the difference of the 3Ddry and the 1D21 simulations because the 3Ddry viscosity is more similar to the 1D20 viscosity than the 1D21 viscosity in West Antarctica. Eventhough the 1D20 simulation is more similar to the 3Ddry simulation than the 1D21, the ice thickness is still underestimated for the Ross and Filchner-Ronne Ice Shelfs when using a 1D rheology. The stabilizing effect increases when using the 3Dwet rheology compared to using the 3Ddry rheology because the viscosity under West Antarctica is even lower. Ice-sheet models using a similar 1D rheology with an upper mantle viscosity of 10^{20} Pa·s or higher and a lithospheric thickness of 100 km (e.g. DeConto et al., 2021; Pollard et al., 2017; Konrad et al., 2015), might therefore underestimate the stability for the Ross and Filchner-Ronne Ice Shelfs.

4 Conclusions and outlook

This study presented the first method to study GIA feedback on ice dynamics for laterally varying viscosity on short timescales of hundreds of years using a coupled ice sheet-3D GIA FE model. Each coupling time steps needs iterations to include the GIA feedback on short timescales of 500 to 5000 years. The coupling method is tested for convergence, which is mainly

dependent on the size of the time step. We concluded that only one iteration per time step is needed if variable coupling time steps of 500 to 5000 years are used. However, three to four iterations over the entire cycle are needed to adjust the initial topography to arrive at the present-day topography at the end of the simulation. Experiments where the resolution in near field and far field are varied indicate that a near field resolution of 30 by 30 km and a far field of 200 by 200 km yields an accuracy

510   of 2 mm/year and a computation time of 5 days to simulate the full glacial cycle.

We created two 3D viscosity models based on an Antarctic-wide seismic model. Using these 3D viscosity models leads to a difference in grounding line position up to 500 km and a difference in ice thickness of up to 2500 meter compared to using a 1D mantle viscosity of 10^{21} Pa·s. The difference in ice thickness between using this 1D rheology and a 3D rheology is 12 times

515   larger than the difference between two realistic 3D rheologies. The ice volume increases with 5 or 7 percent when using a 3D rheology compared to using a 1D viscosity of 10^{20} Pa·s or 10^{21} Pa·s respectively. That is because the low viscosity found in the 3D models leads to large uplift rates which stabilizes the ice sheet more than the 1D rheologies. An ice-sheet model coupled to a 1D rheology with an upper mantle viscosity of 10^{20} Pa·s or 10^{21} Pa·s and lithospheric thickness of 100 meter underestimates the stabilizing effect of GIA. In the future it is desired to apply the coupling method presented in this paper to high resolution

520   models including regional sea level forcing, not only because a higher resolution provides more accurate grounding line simulation, but also because the method converges better since the grid cell is smaller and thus the ice load on one grid cell as well. Furthermore, the effect of sea level variations on the ice shelf melt and on the deformation should be investigated.

The method developed for this study has several advantages which can be exploited in future work when simulation are

525   performed which are as realistic as possible, rather than focussing on the physical principles as we did in this paper. First, the time step is variable throughout the glacial cycle and can be adjusted between iterations of the full glacial cycles. This way, computation time can be saved by simulating the first glacial cycle on a low temporal resolution to obtain the first modelled present-day topography, while the second iteration with the adjusted initial topography can be performed with a higher temporal resolution to include the GIA feedback more accurately. Second, the GIA FE model can be restarted at any time step.

530   Therefore, the last glacial cycle can once be simulated on a very high temporal resolution to obtain present-day results and the coupled model can be restarted from present-day to simulate future evolution of the ice sheet under different scenarios or rheologies. Third, the method has potential for an even higher temporal resolution than used in this study at designated periods in time. For example, the simulation can be restarted at 500 years before present and run on a higher temporal resolution to simulate recent uplift and future climate change projections.

535   **Code and data availability**

The model is momentarily available via the following link: https://figshare.com/s/ffc11d31f0dc355de243. The data underlying this manuscript is accessible via the following link: https://figshare.com/s/fa8cc5dd5a615d8d7662, along with the MATLAB

script to generate the figures included in this manuscript. Once the manuscript is published, the model and the data will be made freely available via the doi 10.4121/19765816 for the model, and the doi 10.4121/19772815 for the data.

540 **Author contribution**

CC and WW designed the method. BdB, BB and CC developed the models used. CC performed the simulations. WW and RW contributed to debugging and the interpretation of the results. CC prepared the manuscript with contributions from all co-authors.

Competing interests

545 The authors declare that they have no conflict of interest.

Acknowledgements

550 **References**

A,G., Wahr, J., and Zhong, S.: Computations of the viscoelastic response of a 3-D compressible Earth to surface loading: an application to Glacial Isostatic Adjustment in Antarctica and Canada. Geophysical Journal International, 192, 557-572, doi:10.1093/gji/ggs030, 2013.

Adhikari, S., Ivins, E.R., Larour, E., Seroussi., H., Morlighem., M., and Nowicki., S.: Future Antarctic bed topography and its
555 implications for ice sheet dynamics. Solid Earth, 5, 569-584, doi:10.5194/se-5-569-2014, 2014.

Albrecht, T., Winkelmann, R., and Levermann, A.: Glacial-cycle simulations of the Antarctic Ice Sheet with the Parallel Ice Sheet Model (PISM) – Part 1: Boundary conditions and climatic forcing. The Cryosphere, 14, 633-656, doi:10.5194/tc-14-599-2020, 2020.

Barletta, V.R., Bevis, M., Smith, B.E., ..., and Smalley, R.: Observed rapid bedrock uplift in Amundsen Sea Embayment
560 promotes ice-sheet stability. Science, 360, 1335-1339, doi:10.1126/science.aao1447, 2018.

Becker, T.W., and Boschi, L.: A comparison of tomographic and geodynamic mantle models. Geochemistry, Geophysics, Geosystems, 3, doi:10.1029/2001GC000168, 2002.

Berends, C.J., de Boer, B., and van de Wal, R.S.W.: Application of HadCM3@ Bristolv1. 0 simulations of paleoclimate as forcing for an ice-sheet model, ANICE2. 1: set-up and benchmark experiments. Geoscientific Model Development, 11, 4657-4675, doi:10.5194/gmd-11-4657-2018, 2018.

Berends, C.J., De Boer, B., Dolan, A.M., Hill, D.J., and Van De Wal, R.S.W.: Modelling ice sheet evolution and atmospheric CO 2 during the Late Pliocene. Climate of the Past, 15, 1603-1619, doi:10.5194/cp-15-1603-2019, 2019.

Bintanja, R., van de Wal, R., and Oerlemans, J.: Modelled atmospheric temperatures and global sea levels over the past million years. Nature, 437, 125–128, doi:10.1038/nature03975, 2005.

Bintanja, R., and van de Wal, R.: North American ice-sheet dynamics and the onset of 100,000-year glacial cycles. Nature, 454, 869–872, doi:10.1038/nature07158, 2008.

Blank, B., Barletta, V., Hu, H., Pappa, F., and van der Wal, W.: Effect of Lateral and Stress-Dependent Viscosity Variations on GIA Induced Uplift Rates in the Amundsen Sea Embayment. Geochemistry, Geophysics, Geosystems, 22, e2021GC009807, doi:10.1029/2021GC009807, 2021.

Bradley, S.L., Reerink, T.J., van de Wal, R.S.W., and Helsen, M.M.: Simulation of the Greenland Ice Sheet over two glacial– interglacial cycles: investigating a sub-ice- shelf melt parameterization and relative sea level forcing in an ice-sheet–ice- shelf model. Climate of the Past, 14, 619–635, doi:10.5194/cp-14-619-2018, 2018.

Bueler, E., Lingle, C.S., and Brown, J.: Fast computation of a viscoelastic deformable Earth model for ice-sheet simulations. Ann. Glaciol., 46, 97–105, doi:10.3189/172756407782871567, 2007.

Bueler, E., and Brown, J.: Shallow shelf approximation as a "sliding law" in a thermomechanically coupled ice sheet model. Journal of Geophysical Research: Earth Surface, 114, F03008, doi:10.1029/2008JF001179, 2009.

De Boer, B., Van De Wal, R.S.W., Lourens, L.J., Bintanja, R., and Reerink, T.J.: A continuous simulation of global ice volume over the past 1 million years with 3-D ice-sheet models. Climate Dynamics, 41, 1365–1384, doi:10.1007/s00382-012-1562-2, 2013.

De Boer, B., Stocchi, P., and Van De Wal, R.S.W.: A fully coupled 3-D ice-sheet-sea-level model: algorithm and applications. Geoscientific Model Development, 7, 2141-2156, doi:10.5194/gmd-7-2141-2014, 2014.

De Boer, B., Stocchi, P., Whitehouse, P.L., and Van De Wal, R.S.W.: Current state and future perspectives on coupled ice-sheet–sea-level modelling. Quaternary Science Reviews, 169, 13-28, doi:10.1016/j.quascirev.2017.05.013, 2017.

DeConto, R.M., Pollard, D., Alley, R.B., Velicogna, I., Gasson, E., Gomez, N., ... and Dutton, A.: The Paris Climate Agreement and future sea-level rise from Antarctica. Nature, 593, 83-89, doi:10.1038/s41586-021-03427-0, 2021.

Fullea, J., Lebedev, S., Martinec, Z., and Celli, N.L.: WINTERC-G: mapping the upper mantle thermochemical heterogeneity from coupled geophysical–petrological inversion of seismic waveforms, heat flow, surface elevation and gravity satellite data. Geophysical Journal International, 226, 146-191, doi:10.1093/gji/ggab094, 2021.

Geruo, A., Wahr, J., Zhong, S.: Computations of the viscoelastic response of a 3-D compressible Earth to surface loading: an application to Glacial Isostatic Adjustment in Antarctica and Canada. Geophysical Journal International, 192, 557–572, doi:10.1093/gji/ggs030, 2013.

Goes, S., Govers, R., and Vacher, A.P.: Shallow mantle temperatures under Europe from P and S wave tomography. Journal of Geophysical Research: Solid Earth, 105, 11153-11169, doi:10.1029/1999JB900300, 2000.

Gomez, N., Mitrovica, J.X., Tamisiea, M.E., and Clark, P.U.: A new projection of sea level change in response to collapse of marine sectors of the Antarctic Ice Sheet. Geophysical Journal International, 180, 623-634, doi:10.1111/j.1365-246X.2009.04419.x, 2010.

Gomez, N., Pollard, D., Mitrovica, J.X., Huybers, P., and Clark, P.U.: Evolution of a coupled marine ice sheet–sea level model. Journal of Geophysical Research: Earth Surface, 117, doi:10.1038/NGEO1012, 2012.

Gomez, N., Pollard, D., and Mitrovica, J.X.: A 3-D coupled ice sheet – sea level model applied to Antarctica through the last 40 ky. Earth and Planetary Science Letters, 384, 88-99, doi:10.1016/j.epsl.2013.09.042, 2013.

Gomez, N., Pollard, D. and Holland, D.: Sea-level feedback lowers projections of future Antarctic Ice-Sheet mass loss. Nature Communications, 6, 8798, doi:10.1038/ncomms9798, 2015.

Gomez, N., Latychev, K., and Pollard, D.: A Coupled Ice Sheet–Sea Level Model Incorporating 3D Earth Structure: Variations in Antarctica during the Last Deglacial Retreat. Journal of Climate, 31, 4041–4054, doi:10.1175/JCLI-D-17-0352.1, 2018.

Gordon, R.B.: Diffusion creep in the Earth's mantle. Journal of Geophysical Research, 70, 2413-2418, doi:10.1029/JZ070i010p02413, 1965.

Han, H.K., Gomez, N., and Wan, J.X.W.: Capturing the interactions between ice sheets, sea level and the solid Earth on a range of timescales: a new "time window" algorithm. Geoscientific Model Development, 15, 1355-1373, doi:10.5194/gmd-15-1355-2022, 2022.

Hay, C.C., Lau, H.C., Gomez, N., ... and Wiens, D.A.: Sea level fingerprints in a region of complex Earth structure: The case of WAIS. Journal of Climate, 30, 1881-1892, doi:10.1175/JCLI-D-16-0388.1, 2017.

Heeszel, D.S., Wiens, D.A., Anandakrishnan, S., ... and Winberry, J.P.: Upper mantle structure of central and West Antarctica from array analysis of Rayleigh wave phase velocities. Journal of Geophysical Research: Solid Earth, 121, 1758-1775, doi:10.1002/2015JB012616, 2016.

Hibbitt, D., Karlsson, B. and Sorensen, P.: Getting Started with ABAQUS, Version (6.14), Hibbitt, Karlsson & Sorensen, Inc, 2016.

Hirth, G., and Kohlstedt, D.: Rheology of the upper mantle and the mantle wedge: A view from the experimentalists. Geophysical Monograph-American Geophysical Union, 138, 83-106, doi:10.1029/138GM06, 2003.

Hu, H., van der Wal, W., and Vermeersen, L.L.A.: A numerical method for reorientation of rotating tidally deformed viscoelastic bodies. Journal of Geophysical Research: Planets, 122, 228-248, doi:10.1002/2016JE005114, 2017.

Ivins, E.R., van der Wal, W., Wiens, D.A., Lloyd, A.J., and Caron, L.: Antarctic upper mantle rheology. Geological Society, London, Memoirs, 56, doi:10.1144/M56-2020-19, 2021.

Karato, S.I., Paterson, M.S., and FitzGerald, J.D.: Rheology of synthetic olivine aggregates: influence of grain size and water. Journal of Geophysical Research: Solid Earth, 91, 8151-8176, doi:10.1029/JB091iB08p08151, 1986.

630 Karato, S.I., Jung, H., Katayama, I., and Skemer, P.: Geodynamic signific.ance of seismic anisotropy of the upper mantle: new insights from laboratory studies. Annual Review of Earth and Planetary Sciences, 36, 59-95, doi:10.1146/annurev.Earth.36.031207.124120, 2008.

Kaufmann, G., Wu, P., and Ivins, E.R.: Lateral viscosity variations beneath Antarctica and their implications on regional rebound motions and seismotectonics. Journal of Geodynamics, 39, 165-181, doi:10.1016/j.jog.2004.08.009, 2005.

635 Kearey, P., Klepeis, K.A., and Vine, F.J.: Global tectonics (3rd ed.). Wiley–Blackwell, 2009.

Kendall, R.A., Mitrovica, J.X., and Milne, G.A.: On post-glacial sea level–II. Numerical formulation and comparative results on spherically symmetric models. Geophysical Journal International, 161, 679-706, doi:10.1111/j.1365-246X.2005.02553.x, 2005.

Konrad, H., Sasgen, I., Pollard, D., and Klemann, V.: Potential of the solid-Earth response for limiting long-term West
640 Antarctic Ice Sheet retreat in a warming climate. Earth and Planetary Science Letters, 432, 254-264, doi:10.1016/j.epsl.2015.10.008, 2015.

Lambeck, K., Rouby, H., Purcell, A., Sun, Y., and Sambridge, M.: Sea level and global ice volumes from the Last Glacial Maximum to the Holocene. PNAS, 111, 15296-15303, doi:10.1073/pnas.1411762111, 2014.

Larour, E., Seroussi, H., Adhikari, S., Ivins, E., Caron, L., Morlighem, M., and Schlegel, N.: Slowdown in Antarctic mass loss
645 from solid Earth and sea-level feedbacks. Science, 364, doi:10.1126/science.aav7908, 2019.

Laskar, J., Robutel, P., Joutel, F., Gastineau, M., Correia, A.C.M., and Levrard, B.: A long-term numerical solution for the insolation quantities of the Earth. Astronomy & Astrophysics, 428, 261-285, doi:10.1051/0004-6361:20041335, 2004.

Lau, H.C., Mitrovica, J.X., Austermann, J., Crawford, O., Al-Attar, D., and Latychev, K.: Inferences of mantle viscosity based on ice age data sets: Radial structure. J. Geophys. Res. Solid Earth, 121, 6991-7012, doi:10.1111/j.1365-
650 246X.2005.02536.x, 2016.

Le Brocq, A.M., Payne, A.J., and Vieli, A.: An improved Antarctic dataset for high resolution numerical ice sheet models (ALBMAP v1). Earth System Science Data, 2, 247-260, doi:10.5194/essd-2-247-2010, 2010.

Le Meur, E., and Huybrechts, P.: A comparison of different ways of dealing with isostasy: examples from modelling the Antarctic Ice Sheet during the last glacial cycle. Annals of Glaciology, 23, 309-317, doi:10.3189/S0260305500013586,
655 1996.

Martin, M.A., Winkelmann, R., Haseloff, M., Albrecht, T., Bueler, E., Khroulev, C., and Levermann, A.: The Potsdam Parallel Ice Sheet Model (PISM-PIK)-part 2: dynamic equilibrium simulation of the Antarctic Ice Sheet. The Cryosphere, 5, 3, 727-740, doi:10.5194/tc-5-727-2011, 2011.

Martin, A.P.: A review of the composition and chemistry of peridotite mantle xenoliths in volcanic rocks from Antarctica and
660 their relevance to petrological and geophysical models for the lithospheric mantle. Geological Society, London, Memoirs, 56, doi:10.1144/M56-2021-26, 2021.

Meredith, M., Sommerkorn, M., Cassotta, S., … Schuur, E.A.G.: Chapter 3: Polar Regions. IPCC SR Ocean and Cryosphere, 2019.

Morland, L.W., and Johnson, I.R.: Steady motion of ice sheets. Journal of Glaciology, 25, 229–246, doi:10.3189/S0022143000010467, 1980.

Morland, L.W.: Unconfined ice-shelf flow. Dynamics of the West Antarctic Ice Sheet, 99–116, doi:10.1007/978-94-0093745-1_6, 1987.

Nield, G.A., Barletta, V.R., Bordoni, A., ... and Berthier, E.: Rapid bedrock uplift in the Antarctic Peninsula explained by viscoelastic response to recent ice unloading. Earth and Planetary Science Letters, 397, 32-41, doi:10.1016/j.epsl.2014.04.019, 2014.

Nield, G.A., Whitehouse, P.L., van der Wal, W., Blank, B., O'Donnell, J.P., and Stuart, G.W.: The impact of lateral variations in lithospheric thickness on glacial isostatic adjustment in West Antarctica. Geophysical Journal International, 214, 811-824, doi:10.1093/gji/ggy158, 2018.

Pan, L., Powell, E.M., Latychev, K., Mitrovica, J.X., Creveling, J.R., Gomez, N., ... and Clark, P.U.: Rapid postglacial rebound amplifies global sea level rise following West Antarctic Ice Sheet collapse. Science Advances, 7, eabf7787, doi:10.1126/sciadv.abf7787, 2021.

Pappa, F., Ebbing, J., Ferraccioli, F., and van der Wal, W.: Modeling satellite gravity gradient data to derive density, temperature, and viscosity structure of the Antarctic lithosphere. Journal of Geophysical Research: Solid Earth, 124, 12053-12076, doi:10.1029/2019JB017997, 2019.

Pattyn, F.: Sea-level response to melting of Antarctic ice shelves on multi-centennial timescales with the fast Elementary Thermomechanical Ice Sheet model (f. ETISh v1. 0). The Cryosphere, 11, 1851-1878, doi:10.5194/tc-11-1851-2017, 2017.

Pattyn, F., and Morlighem, M.: The uncertain future of the Antarctic Ice Sheet. Science, 367, 1331-1335, doi:10.1126/science.aaz5487, 2020.

Pelletier, C., Fichefet, T., Goosse, H., Haubner, K., Helsen, S., Huot, P.V., ... and Zipf, L.: PARASO, a circum-Antarctic fully coupled ice-sheet–ocean–sea-ice–atmosphere–land model involving f. ETISh1. 7, NEMO3. 6, LIM3. 6, COSMO5. 0 and CLM4. 5. Geoscientific Model Development, 15, 553-594, doi:10.5194/gmd-15-553-2022, 2022.

Peltier, W.R. Ice age paleotopography. Science, 265, 195-201, 1994.

Pollard, D., and DeConto, R.: Modelling West Antarctic Ice Sheet growth and collapse through the past five million years. Nature, 458, 329–332, doi:10.1038/nature07809, 2009.

Pollard, D., Gomez, N., and DeConto, R.M.: Variations of the Antarctic Ice Sheet in a coupled ice sheet-Earth-sea level model: sensitivity to viscoelastic Earth properties. Journal of Geophysical Research: Earth Surface, 122, 2124-2138, doi:10.1002/2017JF004371, 2017.

Powell, E.M., Pan, L., Hoggard, M.J., Latychev, K., Gomez, N., Austermann, J., and Mitrovica, J.X.: The impact of 3-D Earth structure on far-field sea level following interglacial West Antarctic Ice Sheet collapse. Quaternary Science Reviews, 273, 107256, doi:10.1016/j.quascirev.2021.107256, 2021.

Reerink, T.J., Van De Berg, W.J., and Van De Wal, R.S.W.: OBLIMAP 2.0: a fast climate model-ice sheet model coupler including online embeddable mapping routines. Geoscientific Model Development, 9, 4111-4132, doi:10.5194/gmd-9-4111-2016, 2016.

700 Scheinert, M., Engels, O., Schrama, E.J., van der Wal, W., and Horwath, M.: Geodetic observations for constraining mantle processes in Antarctica. Geological Society, London, Memoirs, 56, doi:10.1144/M56-2021-22, 2021.

Schoof, C.: Ice sheet grounding line dynamics: Steady states, stability, and hysteresis. Journal of Geophysical Research: Earth Surface, 112, doi:10.1029/2006JF000664, 2007.

Shepard, D.: A two-dimensional interpolation function for irregularly-spaced data. Proceedings-1968 ACM National
705 Conference, 517–524, doi:10.1145/800186.810616, 1968.

Shepherd, A., Ivins, E., Rignot, E., Smith, B., Van Den Broeke, M., Velicogna, I., ... and Wouters, B.: Mass balance of the Antarctic Ice Sheet from 1992 to 2017. Nature, 558, 219-222, doi:10.1038/s41586-018-0179-y, 2018.

Simon, K. M., James, T. S., and Ivins, E. R.: Ocean loading effects on the prediction of Antarctic glacial isostatic uplift and gravity rates. Journal of Geodesy, 84, 305-317, doi:10.1007/s00190-010-0368-4, 2010.

710 Spada, G., Barletta, V.R., Klemann, V., Riva, R.E.M., Martinec, Z., Gasperini, P., et al.: A benchmark study for glacial isostatic adjustment codes. Geophysical Journal International, 185, 106–132, doi:10.1111/j.1365-246x.2011.04952.x, 2011.

Van De Wal, R.S.W., De Boer, B., Lourens, L.J., Köhler, P., and Bintanja, R.: Reconstruction of a continuous high-resolution CO_2 record over the past 20 million years. Climate of the Past, 7, 1459-1469, doi:10.5194/cp-7-1459-2011, 2011.

Van Den Berg, J., Van De Wal, R. S.W., & Oerlemans, J.: A mass balance model for the Eurasian Ice Sheet for the last 120,000
715 years. Global and Planetary Change, 61, 194-208, doi:10.1029/2007JB004994, 2008.

Van Der Wal, W., Wu, P., Wang, H., and Sideris, M.G.: Sea levels and uplift rate from composite rheology in glacial isostatic adjustment modeling. Journal of Geodynamics, 50, 38-48, doi:10.1016/j.jog.2010.01.006, 2010.

Van Der Wal, W., Barnhoorn, A., Stocchi, P., Gradmann, S., Wu, P., Drury, M., and Vermeersen, B.: Glacial isostatic adjustment model with composite 3-D Earth rheology for Fennoscandia. Geophysical Journal International, 194, 61-77,
720 doi:10.1093/gji/ggt099, 2013.

Van Der Wal, W., Whitehouse, P.L., and Schrama, E.J.O.: Effect of GIA models with 3D composite mantle viscosity on GRACE mass balance estimates for Antarctica. Earth and Planetary Science Letters, 414, 134–143, doi:10.1016/j.epsl.2015.01.001, 2015.

Van Der Wal, W., and IJpelaar, T.: The effect of sediment loading in Fennoscandia and the Barents Sea during the last glacial
725 cycle on glacial isostatic adjustment observations. Solid Earth, 8, 955-968, doi:10.5194/se-8-955-2017, 2017.

Weerdesteijn, M., Hu, H., van der Wal, W., and Riva, R.: The potential of numerical modelling for glaciation-induced true polar wander of the Earth. In Geophysical Research Abstracts, 21, ISSN:1029-7006, 2019.

Weihaupt, J.G., Chambers, F.B., van der Hoeven, F.G., and Lorius, C.: Impact crater morphology: The origin of the Mertz and Ninnis Glaciers, Antarctica. Geomorphology, 209, 133-139, doi:10.1016/j.geomorph.2013.11.031, 2014.

730 Whitehouse, P.L., Bentley, M.J., Milne, G.A., King, M.A., and Thomas, I.D.: A new glacial isostatic adjustment model for Antarctica: calibrated and tested using observations of relative sea-level change and present-day uplift rates. Geophysical Journal International, 190, 1464-1482, doi:10.1111/j.1365-246X.2012.05557.x, 2012.

Whitehouse, P.L., Gomez, N., King, M.A., and Wiens, D.A.: Solid Earth change and the evolution of the Antarctic Ice Sheet. Nature communications, 10, 1-14, doi:10.1038/s41467-018-08068-y, 2019.

735 Wu, P.: Using commercial finite element packages for the study of Earth deformations, sea levels and the state of stress. Geophysical Journal International, 158, 2, 401–408, doi:10.1111/j.1365-246X.2004.02338.x, 2004.

Yousefi, M., Wan, J., Pan, L., Gomez, N., Latychev, K., Mitrovica, J. X., Pollard, D., and DeConto, R.M.: The influence of the solid Earth on the contribution of marine sections of the Antarctic Ice Sheet to future sea-level change. Geophysical Research Letters, 49, doi:10.1029/2021GL097525, 2022.